

Tracing titanomagnetite alteration with magnetic measurements at cryogenic temperatures

Andrei Kosterov¹, Leonid Surovitskii,^{1,2} Valerii Maksimochkin,³ Svetlana Yanson¹ and Aleksey Smirnov^{2,4}

¹St Petersburg University, 7-9 Universitetskaya Embankment 199034, St Petersburg, Russia. E-mail: a.kosterov@spbu.ru

²Department of Geological and Mining Engineering and Sciences, Michigan Technological University, 1400 Townsend Drive, Houghton, MI 49931, USA

³Faculty of Physics, Moscow State University, 1, bld. 2 Leninskie Gory 119991, Moscow, Russia

⁴Department of Physics, Michigan Technological University, 1400 Townsend Drive, Houghton, MI 49931, USA

Accepted 2023 September 7. Received 2023 September 6; in original form 2023 June 12

SUMMARY

Titanomagnetite containing up to 0.6–0.7 Ti atoms per formula unit is a primary magnetic mineral phase in submarine basalts and in some terrestrial volcanic rocks. On a geological timescale, it often undergoes alteration, forming new magnetic phases that may acquire (thermo)chemical remanent magnetization. The initial stage of this natural process can be modelled by prolonged laboratory annealing at moderately elevated temperatures. In this study, our goal is to characterize the alteration products resulting from annealing a submarine basalt containing homogeneous titanomagnetite $\text{Fe}_{3-x}\text{Ti}_x\text{O}_4$ ($x \approx 0.46$) at temperatures of 355, 500 and 550 °C for up to 375 hr, by examining their magnetic properties over a wide range of temperatures.

The effect of extended annealing is most apparent in the low-temperature magnetic properties. In the fresh sample, a magnetic transition is observed at 58 K. Below the transition temperature, the field-cooled (FC) and zero-field-cooled (ZFC) saturation isothermal remanent magnetization (SIRM) curves are separated by a tell-tale triangular-shaped area, characteristic for titanomagnetites of intermediate composition. The room-temperature SIRM (RT-SIRM) cycle to 1.8 K in zero field has a characteristic concave-up shape and is nearly reversible. For the annealed samples, the magnetic transition temperature shifts to lower temperatures, and the shape of the curves above the transition changes from concave-up to concave-down. The shape of the RT-SIRM cycles also progressively changes with increasing annealing time. The SIRM loss after the cycle increases up to ~30 per cent for the samples annealed for 375 hr at 355 °C, and for 110 hr at 500 and 550 °C.

The Curie temperatures of the newly formed magnetic phases exceed the Curie temperature of the fresh sample (205 °C) by up to 350 °C. While this effect is most commonly attributed to extensive single-phase oxidation (maghemitization), the behaviour observed at cryogenic temperatures appears incompatible with the known properties of highly oxidized titanomaghemites. Therefore, we propose that, at least in the initial stage of the ‘dry’, that is, not involving hydrothermalism, alteration of titanomagnetite, temperature- and time-controlled cation reordering is the primary mechanism driving changes in both low- and high-temperature magnetic properties.

Key words: Magnetic mineralogy and petrology; Marine magnetism and palaeomagnetism; Rock and mineral magnetism; Titanomagnetite.

1 INTRODUCTION

Titanomagnetite ($\text{Fe}_{3-x}\text{Ti}_x\text{O}_4$, thereafter TMX, where $X = 100-x$) with Ti content x up to 0.6–0.7 is a primary magnetic mineral phase present in submarine basalts and some terrestrial volcanic rocks. On a geological timescale, it is believed to undergo slow

oxidation—a process that is likely widespread and occurs via different mechanisms such as burial heating, baking by intruding magma, hydrothermal alteration, etc. Titanomagnetite alteration results in the acquisition of secondary magnetization in the newly formed magnetic phase(s), producing a potent mechanism for remagnetization. Understanding which magnetic phases, and

in what conditions, are formed during chemical alteration of titanomagnetites is crucial for further assessing how these newly formed phases affect the primary magnetization and distinguish it from possible secondary overprint(s). Since oxidation typically occurs at elevated temperatures, this secondary magnetization can often be classified as thermochemical remanent magnetization (TCRM). TCRM has been the subject of study since the early days of palaeomagnetism (Nagata & Kobayashi 1963; Creer & Petersen 1969; Wasilewski 1969; Kellogg *et al.* 1970), and more recently gained further attention because of its presumably adverse role in absolute palaeointensity determination with the Thellier method (Yamamoto *et al.* 2003; Smirnov & Tarduno 2005; Draeger *et al.* 2006; Yamamoto 2006; Fabian 2009; Shcherbakov *et al.* 2019). However, so far, no clear-cut criteria have been devised for detecting TCRM in rocks. In addition, the laboratory heatings used in Thellier-type (Thellier & Thellier 1959) or Shaw-type (Shaw 1974) palaeointensity experiments often result in additional magneto-mineralogical changes, further complicating data interpretation.

The initial stages of the natural oxidation process may be modelled, to some extent, by prolonged annealing at moderately elevated temperatures. Numerous experiments of this kind have been carried out on synthetic titanomagnetites (Ozima & Larson 1970; Ozima & Sakamoto 1971; Readman & O'Reilly 1972; Keefer & Shive 1980, 1981; Nishitani & Kono 1983, 1989; Brown & O'Reilly 1988), and on rocks bearing titanomagnetites and separated titanomagnetite grains (Creer & Petersen 1969; Ozima & Larson 1970; Marshall & Cox 1971; Johnson & Merrill 1973; Walderhaug *et al.* 1991). The common belief is that annealing of intermediate ($x \geq 0.04$) titanomagnetites at moderate, $< 400^\circ\text{C}$, temperatures, causes vacancies to enter the spinel lattice, forming titanomaghemites. The latter would have considerably higher Curie temperatures than their stoichiometric counterparts and, therefore, could serve as a medium for TCRM acquisition. However, recently an alternative mechanism for Curie temperature enhancement with annealing has been suggested (Bowles *et al.* 2013, 2019; Jackson & Bowles 2018), inferring that the Curie temperature increase in annealed samples is due to increasing ionic order in the spinel lattice.

Magnetic measurements at cryogenic temperatures have been used extensively to characterize both synthetic titanomagnetites (Schmidbauer & Readman 1982; Radhakrishnamurty & Likhite 1993; Moskowitz *et al.* 1998; Carter-Stiglitz *et al.* 2006; Engelmann *et al.* 2010; Church *et al.* 2011; Almeida *et al.* 2014) as well as titanomagnetite/titanomaghemite phases in subaerial (Moskowitz *et al.* 1998; Kosterov 2001; Özdemir & Dunlop 2003; Kosterov *et al.* 2009, 2018; Vigliotti *et al.* 2022) and submarine volcanic rocks (Matzka *et al.* 2003; Doubrovine & Tarduno 2004, 2005, 2006a,b; Krása *et al.* 2005; Krása & Matzka 2007; Wang *et al.* 2021). Intermediate titanomagnetites do not show the Verwey (1939) phase transition at 125 K (Walz 2002), characteristic of stoichiometric magnetite (Aragón *et al.* 1985; Kačol & Honig 1989). Instead, their magnetic properties show an anomalous behaviour in the 30–80 K temperature range manifesting itself in (i) a pronounced loss of remanence given at a temperature below this range after cooling in a zero magnetic field (ZFC); (ii) an even faster decrease of remanence given at a low temperature after cooling in a strong magnetic field (FC) and (iii) a frequency-dependent peak of initial magnetic susceptibility. This behaviour is believed to be caused primarily by sharply decreased magnetocrystalline anisotropy in this temperature range (Syono 1965; Kačol *et al.* 1991).

In this study, we employ magnetic measurements at cryogenic temperatures to evaluate the changes produced by prolonged annealing at 355, 500 and 550 °C in a titanomagnetite-bearing submarine basalt. Our experimental setup mainly pertains to laboratory-produced alteration. However, one may hope that prolonged heating at high temperatures could somewhat emulate alterations occurring naturally at moderately lower temperatures.

2 MATERIALS AND METHODS

Sample P72/4, a submarine basalt (< 500 ka), was dredged from the Holocene bed in the Red Sea during the 30th cruise of the R/V Akademik Kurchatov in 1985. The basalt contains homogeneous titanomagnetite with an approximate TM46 composition and a Curie temperature of 205 °C (Maksimochkin & Grachev 2019). Material from this basalt block has previously been used to model chemical (CRM) and TCRM acquired during annealing at, or slow cooling from, temperatures ranging from 350 to 570 °C (Gribov *et al.* 2019; Shcherbakov *et al.* 2019; Maksimochkin *et al.* 2020; Gribov *et al.* 2021).

To investigate changes induced by prolonged heating in air, we annealed multiple fragments of the sample in a Nabeltherm furnace (Research Centre Geomodel, St. Petersburg State University) for 4, 40, 110, and 375 hr at a nominal temperature of 355 °C, and for 4 and 110 hr at 500 and 550 °C. Once the annealing cycle was complete, the samples were promptly transferred to a shielded room (residual field ~ 400 nT) to allow them to cool naturally.

Micromineralogical studies have been carried out at the Centre for Microscopy and Microanalysis, Science Park of St. Petersburg State University, using a scanning electron microscope (SEM) Quanta 200 3D (FEI, The Netherlands) with an analytical complex Pegasus 4000 (EDAX, USA) in the backscattered and secondary electron modes. For the SEM study, the samples were embedded in epoxy blocks, washed in an ultrasonic bath, dried in a flow dryer, and sprayed with carbon. Electron probe microanalysis was performed on an energy dispersive diffractometer of the Quanta 200 3-D microscope under high vacuum conditions at an accelerating voltage of 15–20 kV.

The temperature dependencies of the mass specific magnetic susceptibility for fresh and annealed fragments have been determined between -192 and 700°C in air and an argon atmosphere using an MFK-1FA susceptibility bridge (AGICO, Czech Republic) connected to the CS-L cryostat and the CS4 furnace. For the fresh sample, susceptibility has been measured in three consecutive cycles to 300, 500 and 700 °C, respectively; for annealed samples, a single cycle to 700 °C has been measured. Hysteresis loops in a maximum field of 7 T and backfield curves of saturation isothermal remanent magnetization (SIRM) acquired in a 5 T field have been measured at 295 K with an MPMS 3 SQUID VSM (Quantum Design, US). For these loops, a paramagnetic correction has been calculated by extrapolating the differential susceptibility dM/dH dependence on $1/H$ to a 20 T field (Starunov *et al.* 2019). Also, hysteresis loops and backfield curves in a 1.8 T maximum field have been measured using a Princeton Measurements Corporation 3900 Model vibrating sample magnetometer (Institute of Physics of the Earth RAS, Moscow). The same instrument was also used to measure first-order reversal curves (FORCs). Between 210 and 340 FORCs with the 1.25 or 1.5 mT uniform field step have been traced depending on the sample. FORC distributions have been computed using a newly developed FORCtool software (<https://forctool.com/>; Surovitskii *et al.* 2022). For the fresh sample, smoothing (SF) and damping (λ) factors for the VARIFORC algorithm (Egli 2013) have been selected

by a trial-and-error search for an optimal solution as outlined in Heslop *et al.* (2020). FORC distributions for the annealed samples have been calculated with the same SF and damping factor as for the fresh sample for the sake of consistency; however, these may not be optimal in the sense of Heslop *et al.* (2020).

Low-temperature magnetic measurements have been carried out at the Centre for Diagnostics of Functional Materials for Medicine, Pharmacology and Nanoelectronics, Science Park of St. Petersburg State University. Magnetization measurements carried out using an MPMS 3 SQUID VSM included the following. SIRM acquired in a 5 T field at 1.8 K after cooling at zero (zero-field cooling, ZFC) and in a strong (5 T, field cooling, FC) magnetic field, have been traced during warming to 300 K in a zero field. SIRM (5 T) acquired at 300 K (referred to thereafter as RT-SIRM) has been measured during a cooling–warming cycle between 300 and 1.8 K, also in a zero field. All measurements have been carried out in the vibration magnetometer mode with the temperature change rate of 2 K min⁻¹, allowing to record the magnetic moment value every 0.05 K. The temperature and frequency dependencies of the mass specific complex magnetic susceptibility $k = k' - i \cdot k''$, where k' and k'' are the in-phase and out-of-phase susceptibilities, respectively, have been determined between 2 and 300 K at 2 K increment between 2 and 80 K, and 5 K between 80 and 300 K, using a PPMS instrument (Quantum Design). Measurements have been performed in a driving field of 250 μ T at seven frequencies between 11 and 9500 Hz selected so that the increment in log frequency would be approximately uniform.

3 RESULTS

3.1 Characterizing fresh P72/4 sample

Backscatter electron (BSE) imaging of the fresh sample reveals the presence of skeletal titanomagnetite grains typical for rapidly cooled submarine basalts (Fig. 1a). No exsolution structures within the grains were observed. However, the fine size of titanomagnetite grains did not allow one to determine their precise composition from microprobe data. Magnetic hysteresis properties (Fig. 1b and Table 1) indicate that the sample is in a pseudo-single domain (PSD) magnetic state. Worth noting is a relatively low value of H_{cr}/H_c of 1.25, which is sometimes encountered in submarine basalts (Gee & Kent 1999). The central part of the FORC diagram (Fig. 1c) has an arrowhead shape centred at about 15 mT, while the outer contours are clearly onion-like, the 90 per cent density contour extending to about 55 mT along the $\mu_0 H_c$ axis. Both features are characteristic of small PSD grains (Roberts *et al.* 2014). The maximum of the hysteron distribution appears to be slightly, by about 1.2 mT, displaced down relative to the $\mu_0 H_b = 0$ line, suggesting that magnetostatic interactions are non-negligible in this sample. This is a well-known property of strongly interacting magnetic particles such as those used in magnetic recording media (Pike *et al.* 1999), considered as an indication of a negative mean interaction field. In addition, an increased hysteron density in the vicinity of the $\mu_0 H_b$ axis may also be due to interactions (Muxworthy *et al.* 2006). Indeed, non-negligible magnetostatic interactions are expected to act between the close segments of abundant skeletal titanomagnetite grains as revealed by BSE images (Fig. 1a).

Measurements on duplicate specimens show that the concentration of the ferrimagnetic phase in the rock can vary within ± 15 per cent of the mean value, as attested by the respective saturation magnetization values. At the same time, the M_{rs}/M_s ratio, coercive force,

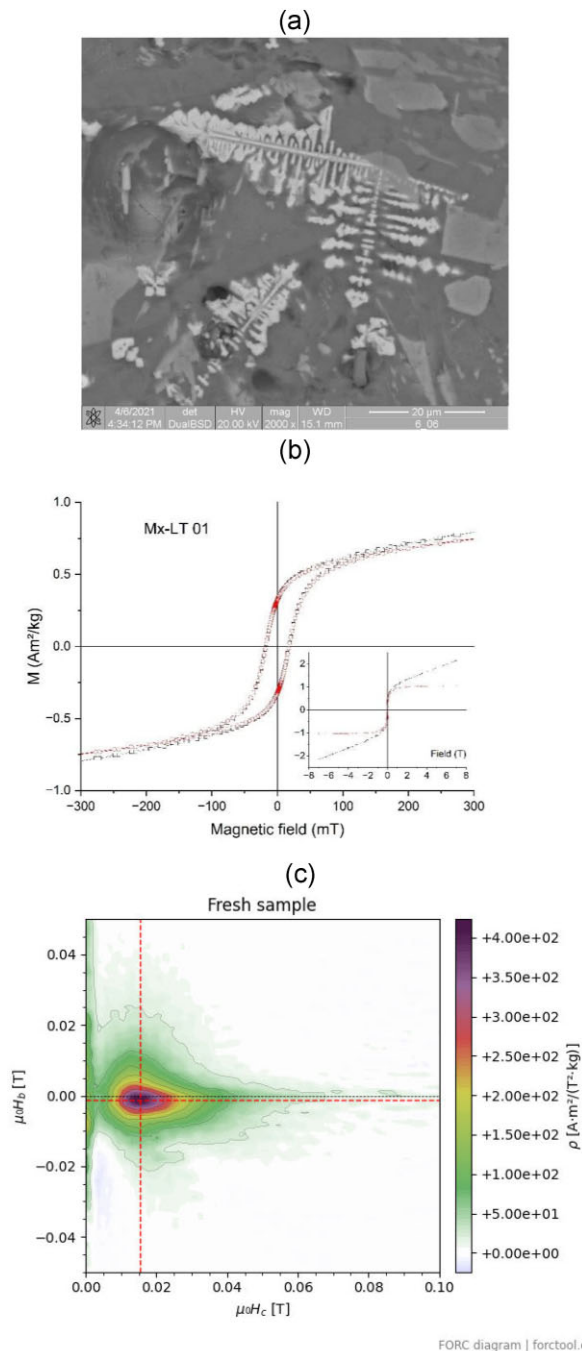


Figure 1. P72/4 fresh sample. (a) Backscattered electron image of a titanomagnetite grain; (b) central part of a hysteresis loop measured at 295 K in a 7 T maximum field. The measured loop is shown in black, corrected for high-field slope according to the extrapolation method of Starunov *et al.* (2019) in red. Inset shows full ± 7 T loops; (c) FORC distribution (smoothing factors, $SF_c = SF_b = 2$ and damping factors, $\lambda_c = \lambda_b = 0.04$). Contours are drawn every 10 per cent of maximum hysteron density. Bold dashed lines mark the location of the maximum.

coercivity of remanence, and coercivity ratio H_{cr}/H_c are constant within 1 per cent. The basalt sample can thus be considered sufficiently homogeneous to justify comparison of the results obtained by annealing different duplicate specimens.

The temperature dependence of low-field susceptibility determined on a fresh sample in argon show that the sample is stable up

Table 1. Parameters of hysteresis loops measured in a maximum field of 7 T at 295 K, for the fresh and annealed samples of P72/4 submarine basalt. The last two columns list the coordinates of the FORC distribution maxima.

Sample	M_s (Am ² kg ⁻¹)	M_{rs} (Am ² kg ⁻¹)	M_{rs}/M_s	$\mu_0 H_c$ (mT)	$\mu_0 H_{cr}$ (mT)	H_{cr}/H_c	$\mu_0 H_{c, FORC}$ (mT)	$\mu_0 H_{u, FORC}$ (mT)
Fresh sample								
No. 1 Fresh	1.035	0.3223	0.3114	17.70	22.24	1.257	15.5	-1.20
No. 2 Fresh	1.211	0.3761	0.3106	17.18	21.55	1.254		
No. 3 Fresh	0.9434	0.3036	0.3218	17.31	21.63	1.250		
Annealed at 355 °C								
4 hr	1.202	0.3423	0.2848	15.26	19.91	1.305	13.1	-1.44
40 hr	1.370	0.3285	0.2398	12.74	17.98	1.411	10.2	-0.94
110 hr	1.390	0.3112	0.2239	12.57	18.72	1.489	11.9	-0.24
375 hr	1.320	0.2834	0.2147	14.29	22.88	1.601	13.1	-0.94
Annealed at 500 °C								
4 hr	1.290	0.4208	0.3262	29.37	40.91	1.392	27.6	-2.07
110 hr	1.437	0.4838	0.3367	42.70	60.42	1.415	50.5	-2.80
Annealed at 550 °C								
4 hr	1.410	0.5400	0.3830	49.14	63.29	1.288	51.2	-3.30
110 hr	1.092	0.3317	0.3038	37.08	54.28	1.464	39.2	-2.40

to 500 °C (Fig. 2a), in agreement with the previous work (Maksimochkin & Grachev 2019). The Curie temperature, evaluated from the minimum of the derivative of the warming curve to 300 °C, is 205 °C. When heated to 700 °C, a minor phase with the Curie temperature of ~550 °C is seen in both heating and cooling curves. While it is impossible to determine whether this phase is primary or forms due to heating, its contribution to the magnetic properties of the sample is negligible. On the contrary, when heated in air, the sample (fresh aliquot was used) begins to alter between 350 and 400 °C, and after heating to 500 °C produces two distinct magnetic phases with Curie temperatures of about 480 and 300 °C (Fig. 2b). Further heating to 700 °C transforms these two phases into a single phase with a Curie temperature of ~550 °C and possibly also into a continuous range of phases with Curie temperatures down to 400 °C.

For fresh P72/4 material, the ZFC and FC remanences exhibit rather complex behaviour (Figs 3a and b). About a quarter of these is demagnetized already at 5 K. This property, albeit less pronounced, has previously been observed in subaerial volcanic rocks containing titanomagnetites with compositions ranging from pure magnetite to approximately TM10-15 (Kosterov 2001; Kosterov *et al.* 2009). It may be due to a mineral with very low magnetic ordering temperature, or else to extremely fine superparamagnetic grains. The titanomagnetite phase manifests itself in a magnetic transition at 58 K. Below this temperature, the FC and ZFC curves sharply diverge, as observed for titanomagnetites of intermediate composition (Kosterov *et al.* 2009, 2018; Almeida *et al.* 2014; Wang *et al.* 2021; Vigliotti *et al.* 2022). Also, an accelerated magnetization decay at 30–35 K is observed in the FC curve (see the derivative curve dFC/dT , Fig. 3b). The origin of this feature remains unclear.

The in-phase AC magnetic susceptibility k' (Fig. 3c) shows a fivefold decrease up to *ca.* 50 K, apparently due to the contribution of the paramagnetic mineral matrix. Between 50 and 150 K, frequency-dependent behaviour is seen, manifesting itself also in the characteristic peaks of the out-of-phase susceptibility (Fig. 3d). Similar behaviour has been observed for synthetic titanomagnetites (Radhakrishnamurthy & Likhite 1993; Church *et al.* 2011) and more recently also in titanomagnetite-bearing rocks (Kosterov *et al.* 2018; Wang *et al.* 2021; Vigliotti *et al.* 2022).

3.2 Samples annealed at 355 °C

Fig. 4 summarizes temperature dependencies of magnetic susceptibility measured in argon atmosphere for the samples annealed at 355 °C. Annealing for only 4 hrs already results in the formation of new magnetic phases (phases 1 and 2 thereafter) with Curie temperatures of 420 and 590 °C, respectively (Fig. 4a). At the same time, a phase close to the initial titanomagnetite survives in a notable amount, although its Curie point also shifts towards high temperatures (Figs 4a and e). With increasing annealing duration, the initial titanomagnetite completely disappears, the Curie temperature of phase 1 increases, reaching 500 °C after 375-hr annealing, and the Curie temperature of phase 2 remains largely unchanged (Figs 4b–d). Phase 1 is however unstable to heating to 700 °C in argon, which reduces it to essentially the initial titanomagnetite in samples annealed for up to 110 hr (Fig. 4f). In the sample annealed for 375 hr, the complete reduction of the initial titanomagnetite is not reached, traces of phase 1 remain, and the Curie temperature of the reduced phase is 250 °C, rather than 205 °C. The newly formed phase 2 survives the heating to 700 °C almost unchanged.

The parameters of the hysteresis loops for the annealed samples are listed in Table 1, and plotted on a Day–Dunlop diagram (Fig. 5). FORC diagrams for samples annealed at 355 °C are shown in Fig. 6. Increasing annealing time results in a gradual decrease of M_{rs}/M_s and a matching increase of H_{cr}/H_c ratio. Bearing in mind that grains are unlikely to grow physically during annealing, this could be due to relieving internal stress initially present in the fresh material. Along the same line, inspection of FORC diagrams shows that at the first stages of annealing, hysteron density distribution narrows, so that for the sample annealed for 40 hr, the 90 per cent density contour only reaches about 45 mT (Fig. 6b) as compared to 65 mT for the fresh sample. In contrast, at longer annealing times the whole hysteron distribution expands significantly (Figs 6c and d), suggesting that magnetostatic interactions grow with increasing annealing time. Increase of interactions would also explain the progressive reducing of the bulk coercive force for the samples annealed for 110 and 375 hr. Overall, it may be hypothesized that upon the increase of the annealing duration, single-domain-like magnetic states would have an ample amount of time to relax into a more PSD-like states, enhancing the hysteron density close to the $\mu_0 H_b$ axis (Figs 6c and d).

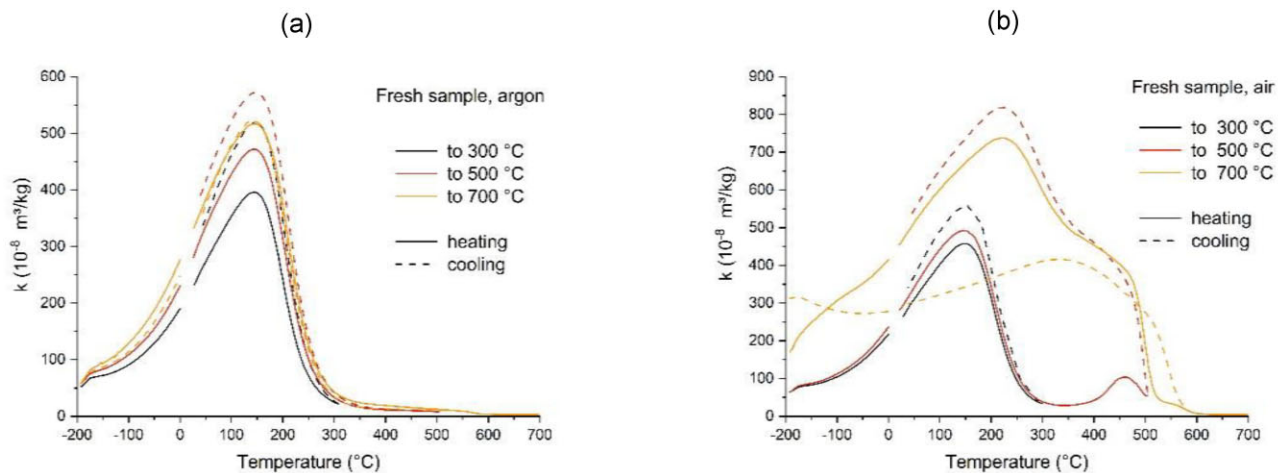


Figure 2. Magnetic susceptibility cycles for the fresh P72/4 sample to 300, 500 and 700 °C in (a) argon atmosphere and (b) in air.

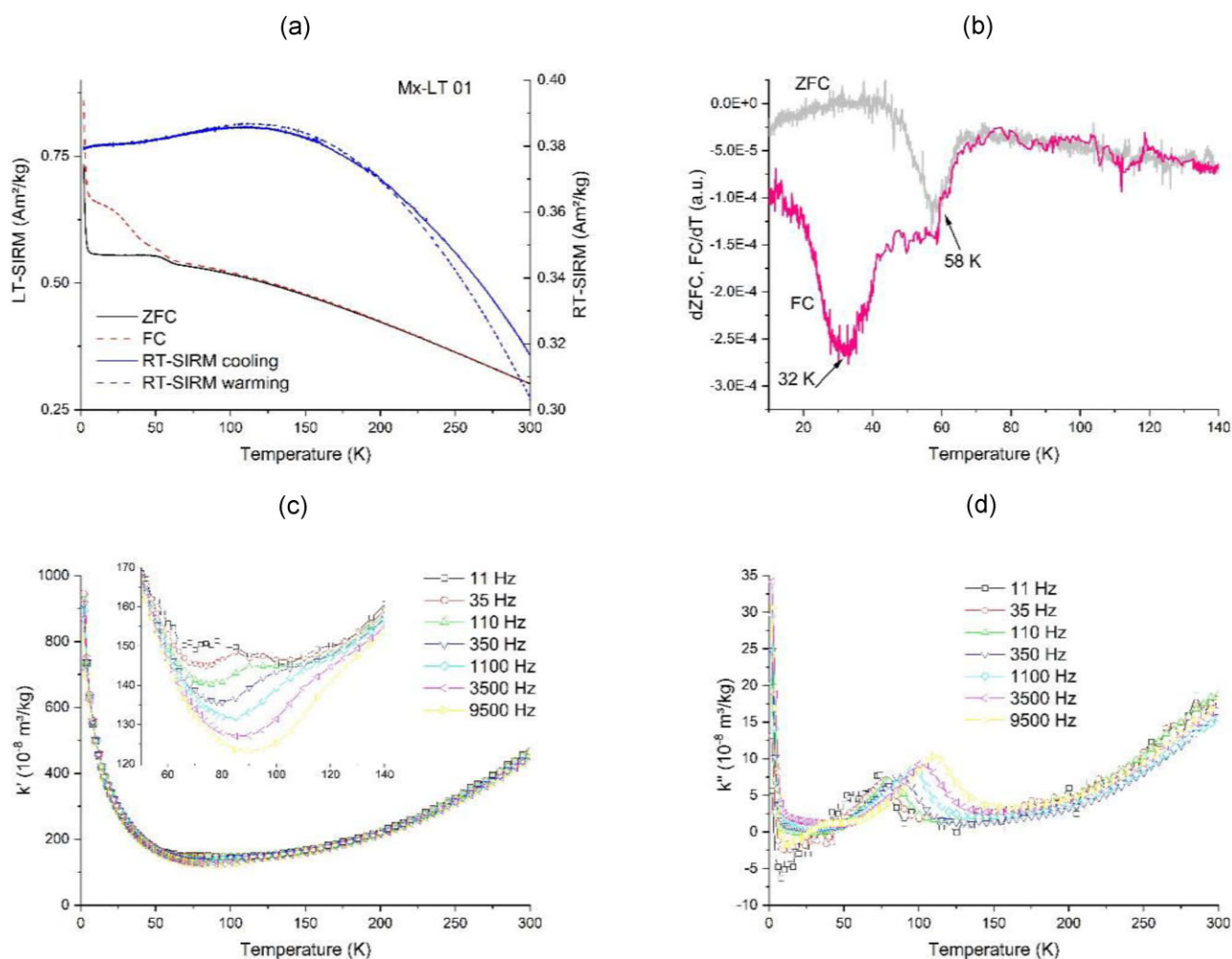


Figure 3. Magnetic properties of the fresh P72/4 sample at cryogenic temperatures. (a) Decay of SIRM given at 1.8 K after ZFC and FC (5 T), respectively, on warming in a zero field (black and red curves, left ordinate axis), and a zero-field cycle of SIRM given at 300 K (blue curve, right ordinate axis). Note the different scales on the two ordinates axes. (b) Derivatives of ZFC and FC SIRM decay curves showing magnetic transitions at 58 and 32 K (FC curve only). Derivative curves are presented as 51-point adjacent averages. (c) and (d) Temperature dependencies of the in-phase and out-of-phase AC magnetic susceptibility, respectively, measured at seven frequencies between 11 and 9500 Hz. Inset in (c) shows a detailed view of frequency-dependent behaviour between 50 and 140 K.

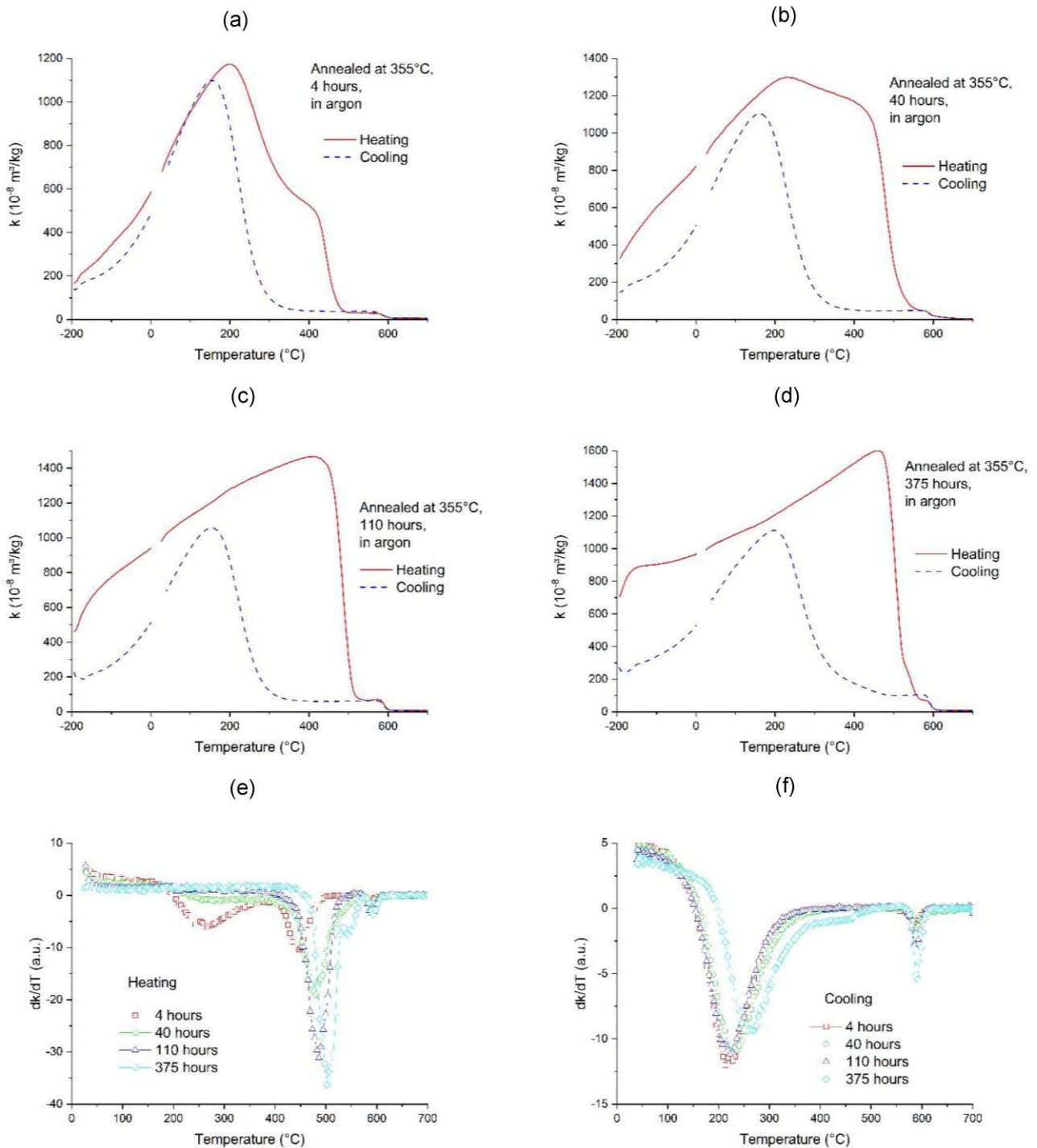


Figure 4. (a)–(d) Temperature dependencies of magnetic susceptibility for samples annealed at 355 °C for 4, 40, 110 and 375 hr, respectively, and derivatives of (e) heating and (f) cooling curves showing the evolution of Curie temperatures with increasing annealing time.

The effect of prolonged annealings is clearly seen in low-temperature magnetic properties. For the annealed samples, the shape of the ZFC and FC SIRM demagnetization curves and the ratio between them (Fig. 7) remain similar to those observed for the fresh sample, but with some notable differences. At the initial annealing stage (4 hr), the 58 K transition in the ZFC curve shifts to about 50 K, and a second transition emerges at about 40 K. On further annealing, the two transitions coalesce into a single one at 45 K. The magnetization decay rate below the transition gradually increases (Figs 7e and f). In the FC curves, the magnetic

transition at 30–35 K gradually disappears with annealing, leaving the single transition at 45 K. The shape of the demagnetization curves above the transition changes from concave up to concave down, as illustrated by their temperature derivative curves changing the slope above *ca.* 60 K from initially negative to near-zero for 110 hr annealing time and further to positive for 375 hr (Figs 7e and f).

The RT-SIRM cycle to 1.8 K in the zero field for the fresh sample has a characteristic convex shape and is almost reversible. Magnetization at 1.8 K is about 20 per cent higher than the initial value

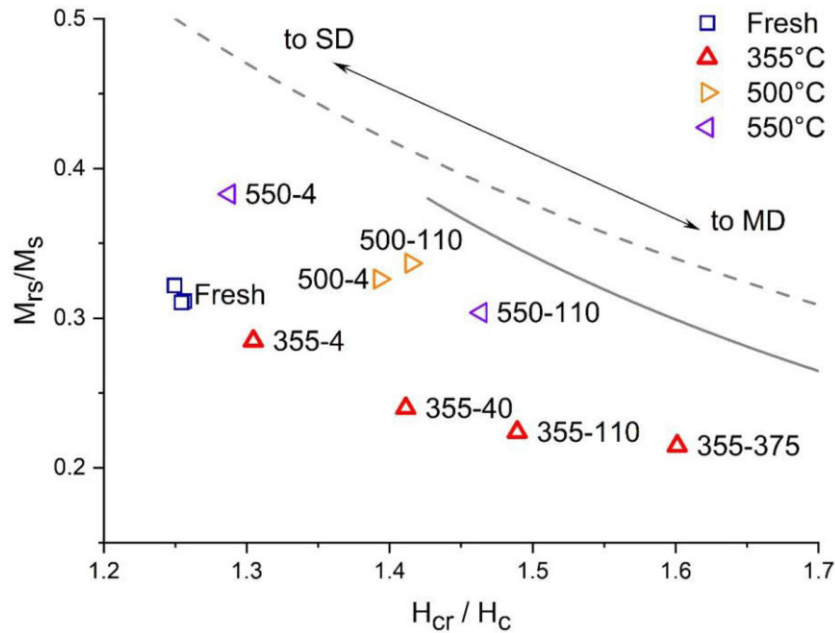


Figure 5. Extended view of Day plot (Day *et al.* 1977), showing figurative points for fresh and annealed samples. The first number on the labels is the annealing temperature in °C, second is the annealing time in hours. Solid and dashed lines are SD–MD mixing lines for magnetite (Dunlop 2002). Arrow marks directions towards parameter ranges corresponding to SD and MD grains, respectively.

at 300 K, and magnetization loss after the cycle is only 2–3 per cent. With increasing annealing time, the shape of RT-SIRM cycles changes progressively and the irreversibility degree (defined here as a loss of SIRM given at 300 K after a cycle to 1.8 K in a zero field) increases to about 30 per cent for the sample annealed for 375 hr, in agreement with magnetic softening seen in hysteresis properties.

In contrast to the remanence, the change in AC magnetic susceptibility due to annealing manifests itself most strongly above 50 K, where the temperature dependencies of the in-phase susceptibility k' change the shape dramatically (Figs 8a, c, e and g), remaining, however, frequency-dependent between 50 and 150 K. Somewhat surprisingly, characteristic peaks of the out-of-phase susceptibility occur at nearly the same temperatures for all annealing times, gradually increasing in intensity (Figs 8b, d, f and h).

3.3 Samples annealed at 500 and 550 °C

Annealing at 500 and 550 °C for 4 hr produces two magnetic phases with Curie temperatures of about 500 and 560–570 °C (Figs 9a, c, e and g). At a more prolonged annealing for 110 hr at the same two temperatures, a seemingly single phase is produced with Curie temperatures of 575 and 550 °C, respectively. However, the annealed samples are not entirely stable to heating to 700 °C in an argon atmosphere. For samples annealed for 4 hr, Curie temperature determined from the cooling curves is significantly lower than those obtained from the heating curves (compare Figs 9e and g, and 9f and h). In samples annealed for 110 hr, a single phase seen in heating curves disintegrates into two phases with close but distinct Curie temperatures on cooling.

FORC diagrams for samples annealed at 500 and 550 °C are shown in Fig. 10. All diagrams extend to nearly 150 mT along the $\mu_0 H_c$ axis, more than twice compared to those measured for the fresh sample and samples annealed at 355 °C. The spread of

the FORC distribution along the $\mu_0 H_b$ axis is also notably larger, whereas the downward shift of the distribution maximum relative to the $\mu_0 H_c = 0$ line increases. Overall, hysteron density distribution appears more single-domain-like in these samples, in line with considerably enhanced coercive force and coercivity of remanence (compare Figs 1c and 5, on one hand, and Fig. 10 on the other). Increased downward shift of the distribution maximum with respect to the $\mu_0 H_c = 0$ line may indicate a more significant magnetostatic interaction between SD-like regions. However, the details vary depending on the annealing temperature. At 500 °C, coercivity increases with annealing time and the M_{rs}/M_s ratio changes only slightly compared to the fresh sample, while at 550 °C both the M_{rs}/M_s ratio and coercivity are maximal after 4 hr of annealing and decrease considerably after 110 hr of annealing.

The properties at cryogenic temperatures exhibit progressive changes with annealing temperature and duration. The magnetic transition shifts to still lower temperatures, 38–39 K for the samples annealed at 500 °C, and 34–36 K for those annealed at 550 °C (Fig. 11). The difference between the ZFC and FC curves persists, but the slope of the ZFC curve below the transition is significantly greater than for the samples annealed at 355 °C. The sample annealed at 500 °C for 110 hr also exhibits a broad Verwey transition centred at 95 K, indicating that in this case, the newly formed phase is close to magnetite. Zero-field RT-SIRM cycles develop fairly strong irreversibility, similar to that previously observed in rocks containing titanomagnetite of TM10–TM30 composition (Kosterov *et al.* 2009, 2018).

The shape of susceptibility temperature dependencies in the 2–300 K range evolves to develop well-pronounced frequency-dependent maxima of the in-phase susceptibility (Figs 12a, c, e and f). On the other hand, the maxima of the out-of-phase susceptibility (Figs 12b, d, f and h) decrease in magnitude and shift to considerably lower temperatures (*ca.* 45–60 K) compared to the samples annealed at 355 °C.

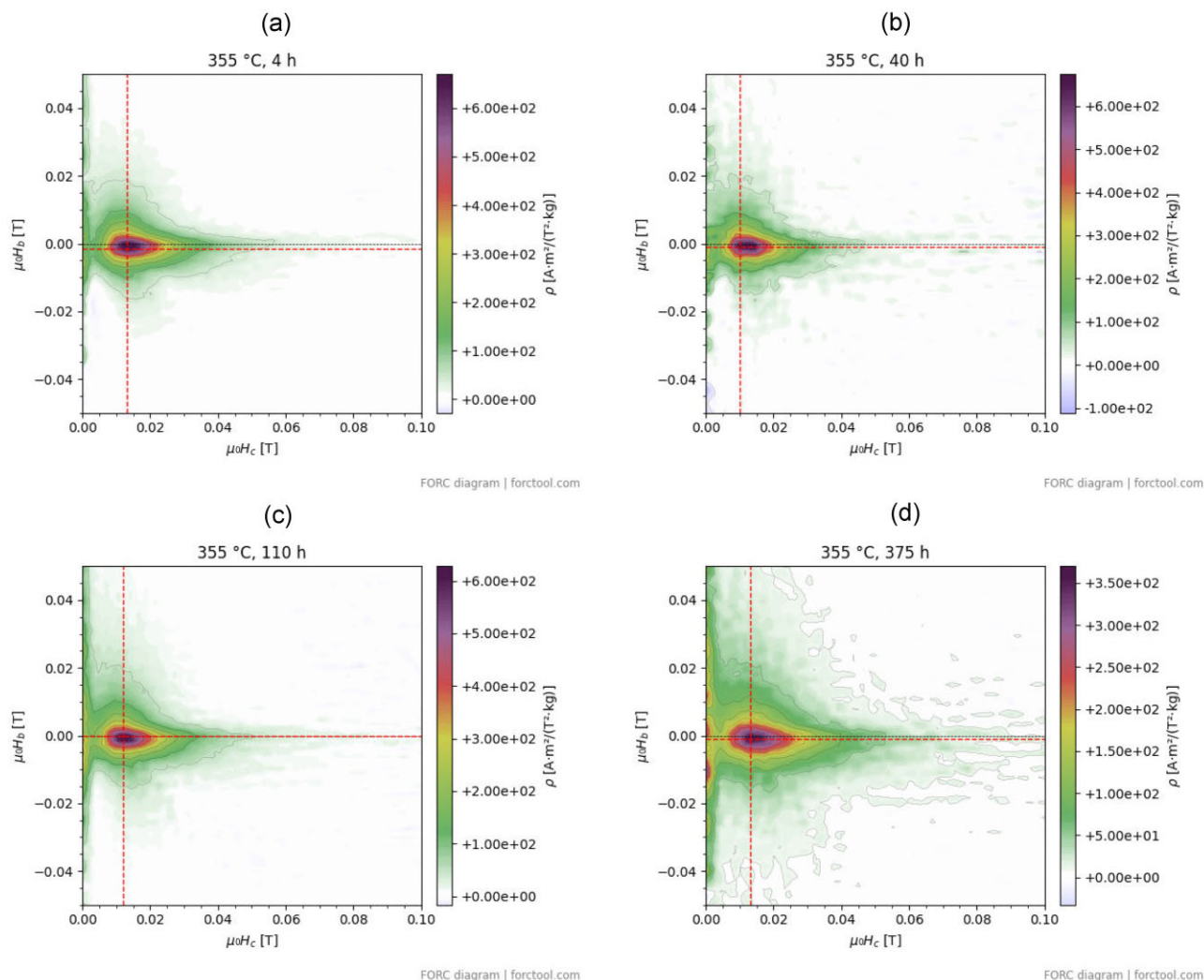


Figure 6. FORC distributions for samples annealed at 355 °C. Smoothing factors, $SF_c = SF_b = 2$ and damping factors, $\lambda_c = \lambda_b = 0.04$ have been used to calculate all distributions. Contours are drawn every 10 per cent of maximum hysteresis density. Dashed lines mark the location of the maximum.

4 DISCUSSION

4.1 Low-temperature magnetic properties of intermediate titanomagnetites

Temperature-dependent behaviour of remanence and AC magnetic susceptibility in magnetic materials is governed by several factors, of which magnetic phase transitions, if present, are by far the most significant (*cf.* Dunlop & Özdemir 1997). Temperature variation of the intrinsic material properties such as magnetocrystalline anisotropy and magnetostriction also plays an essential role. All of these factors are, in turn, affected by the stoichiometry of the material and the degree of crystallinity. On top of this, the low-temperature variation of remanence and magnetic susceptibility is in most cases grain-size dependent.

Titanomagnetites $Fe_{3-x}Ti_xO_4$ with $x > 0.035$ do not exhibit the Verwey transition (Kozłowski *et al.* 1996), resulting in a major change in their low-temperature magnetic behaviour, compared to magnetite. The signature of the Verwey transition disappears from demagnetization curves of remanence given below the transition temperature (typically, 2–20 K); however, irreversibility of zero-field cycles of remanence given at 300 K persists in some cases

(Özdemir & Dunlop 2003; Kosterov *et al.* 2009, 2018) though not universally (*cf.* Wang *et al.* 2021). This behaviour may be due to the temperature dependence of the magnetocrystalline anisotropy that remains qualitatively similar to that of magnetite for a wide range of compositions, approximately up to $x \sim 0.4$. For such titanomagnetites, the first constant of magnetocrystalline anisotropy K_1 is negative at 300 K. Upon temperature decrease, its absolute value first increases and then starts to decrease, approaching zero at the so-called isotropic point. With increasing Ti content, the isotropic point temperature first shifts toward lower temperatures, to below 77 K for the material with $x = 0.18$ – 0.36 (Syono 1965; Kačol *et al.* 1991), and then starts to increase again, so that titanomagnetite with the nominal composition TM41 has an isotropic point of about 125 K, very close to that of magnetite (Kačol *et al.* 1991). For still more Ti-rich compositions, K_1 turns positive at all temperatures below 300 K (Syono 1965; Kačol *et al.* 1991), and is strongly temperature-dependent increasing sharply to very high values below 200 K.

The variation of magnetostriction with temperature for intermediate titanomagnetites is known only in the 100–300 K range (Klerk *et al.* 1977). Unlike that of the magnetocrystalline anisotropy, temperature dependence of magnetostriction changes significantly

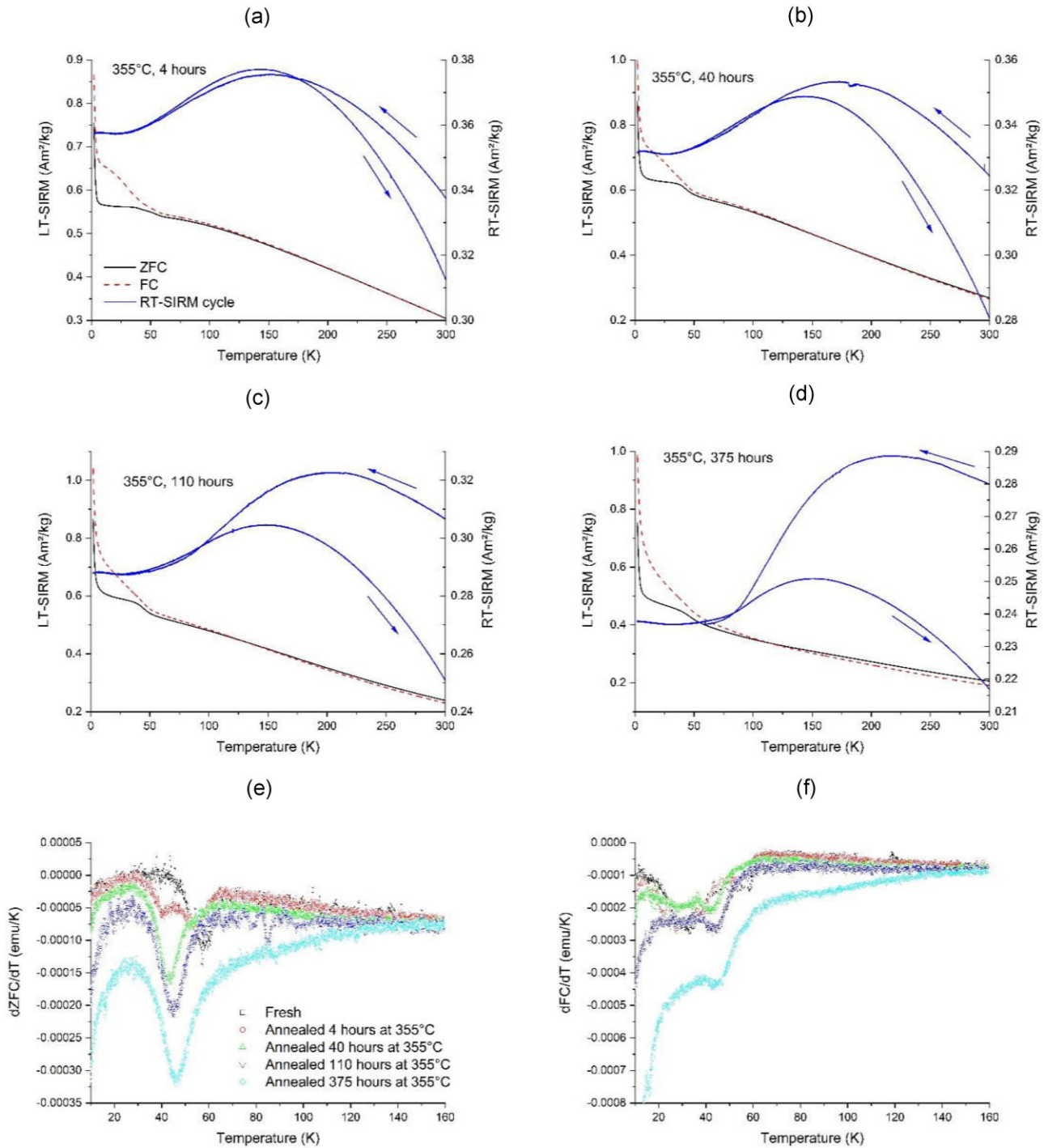


Figure 7. (a)–(d) Decay of SIRM given at 1.8 K after ZFC and FC (5 T), respectively, on warming in a zero field (black and red curves, left ordinate axis), and a zero-field cycle of SIRM given at 300 K (blue curve, right ordinate axis) for samples annealed at 355 °C. Note the different scales on the two ordinate axes. Annealing time is indicated in the figures. (e) and (f) Evolution of derivative curves of ZFC and FC SIRM decay, respectively, with increasing annealing time. Derivative curves for the fresh sample are plotted for reference. Derivative curves are presented as 51-point adjacent averages.

with increasing Ti content. Both λ_{100} and λ_{111} constants rapidly increase and develop a notable temperature dependence for compositions with $x > 0.2$. For example, at 100 K, λ_{111} is a factor of 5, and λ_{100} is a factor of 20 higher for TM40 titanomagnetite than for magnetite. Magnetostriction is considered to be a primary factor that controls the magnetic behaviour of both magnetite- (Hodych 1982a) and TM60-bearing rocks (Hodych 1982b) between 100 and 300 K. Therefore, it may be inferred

that the properties of the fresh P72/4 sample containing titanomagnetite of an average TM46 composition are also governed by magnetostriction.

ZFC/FC remanence decay curves of the fresh P72/4 basalt show a characteristic pattern. Below the magnetic transition, which in our case occurs at 58 K, the remanence in the FC state is considerably higher than the remanence in the ZFC state, but decreases with increasing temperature at a much higher rate. As a result,

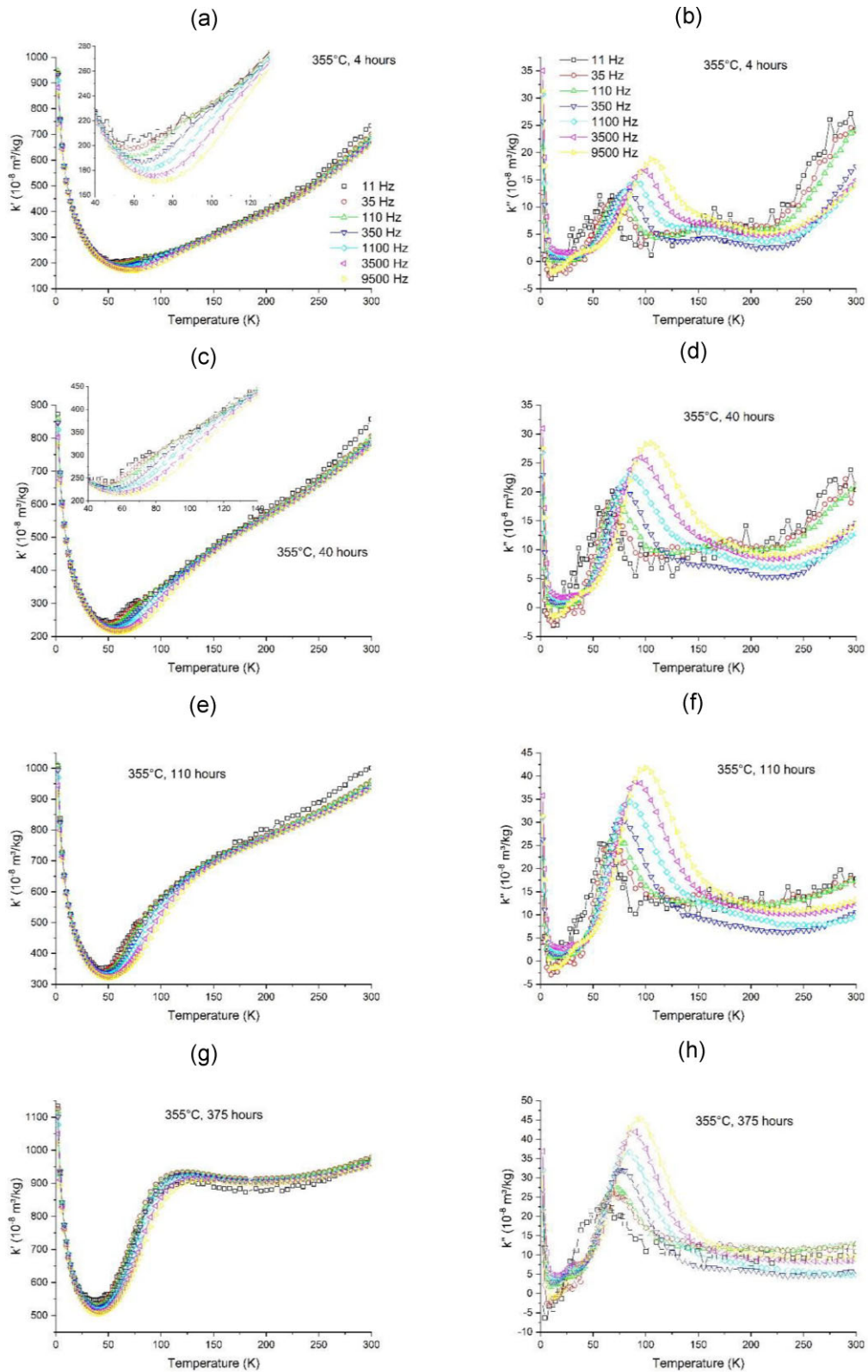


Figure 8. Temperature dependencies of (a), (c), (e) and (g) in-phase and (b), (d), (f) and (h) out-of-phase AC magnetic susceptibility measured at seven frequencies between 11 and 9500 Hz for samples annealed at 355 °C. Annealing time is (a) and (b) 4 hr, (c) and (d) 40 hr, (e) and (f) 110 hr and (g) and (h) 375 hr. Insets in (a) and (c) show detailed views of frequency-dependent behaviour.

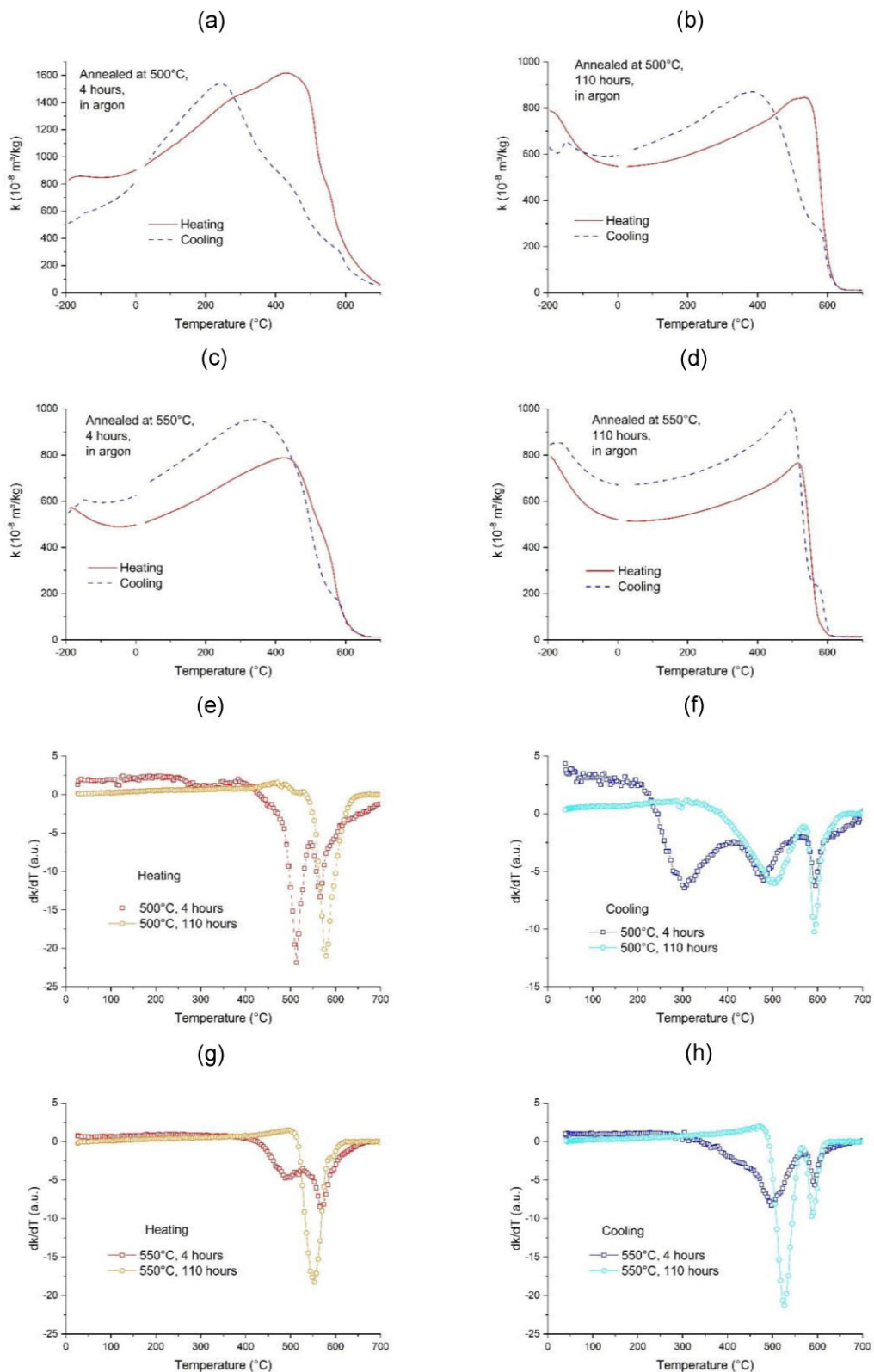


Figure 9. (a) and (b) Temperature dependencies of magnetic susceptibility for samples annealed at 500 °C for 4 and 110 hr, respectively; (c) and (d) the same for samples annealed at 550 °C; (e) and (f) derivatives of heating and cooling susceptibility curves for samples annealed at 500 °C for 4 and 110 hr, respectively and (g) and (h) the same for samples annealed at 550 °C.

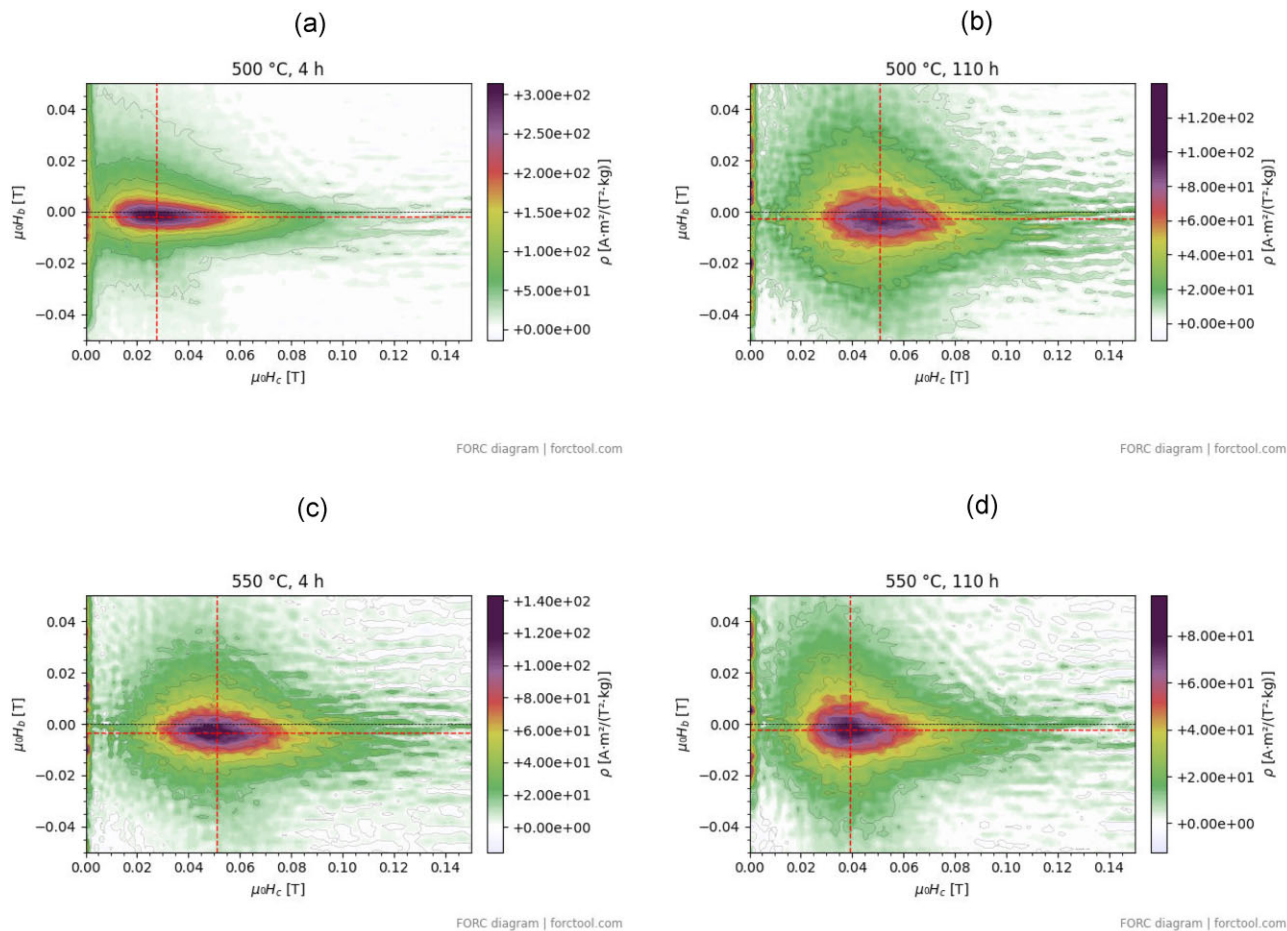


Figure 10. FORC distributions for samples annealed at (a) and (b) 500 °C and (c) and (d) 550 °C. Smoothing factors, $SF_c = SF_b = 2$ and damping factors, $\lambda_c = \lambda_b = 0.04$ have been used to calculate all distributions. Contours are drawn every 10 per cent of maximum hysteron density. Dashed lines mark the location of the maximum.

the area between the FC and ZFC remanence decay curves has a recognizable triangular shape. This behaviour has previously been observed in synthetic titanomagnetites (Almeida *et al.* 2014) and in titanomagnetite-bearing rocks (Kosterov *et al.* 2009, 2018; Wang *et al.* 2021). It should be noted that Curie temperatures of these samples vary widely, from < 200 °C (Sample S3 of Almeida *et al.* 2014 and Sample 39I-TVG02 of Wang *et al.* 2021) to > 500 °C (Sample P15 of Kosterov *et al.* 2009), implying that the above pattern only weakly depends on the composition of titanomagnetite. However, it seems that in more Ti-rich titanomagnetites the decay rate of ZFC remanence is lower than in their Ti-poor counterparts (compare, e.g. our P72/4 sample and sample 39I-TVG02 of Wang *et al.* 2021), but this observation needs further confirmation on a larger number of samples.

Unlike the remanence given at a low temperature, zero-field 300 K—LT—300 K SIRM cycles of intermediate titanomagnetites show a variety of behaviours, from nearly reversible (sample P15, Kosterov *et al.* 2009; sample S3, Almeida *et al.* 2014; sample 39I-TVG02, Wang *et al.* 2021; sample P72/4, this study) to highly irreversible (e.g. sample S2, Almeida *et al.* 2014; most samples in Kosterov *et al.* 2018). Again, there seems to be a trend that more Ti-rich samples show a higher degree of reversibility, but it is by no means universal, as demonstrated by the example of sample P15 having the Curie temperature of 535 °C (Kosterov *et al.* 2009). With increasing Ti content in titanomagnetite, magnetostriction increases faster than magnetocrystalline anisotropy. It may be conjectured therefore that

in more Ti-rich titanomagnetites magnetostriction is a dominant factor controlling remanence behaviour at cryogenic temperatures. However, if stress is sufficiently high, magnetostriction may govern remanence even in relatively Ti-poor titanomagnetite, like one in the P15 sample of Kosterov *et al.* (2009). Given the above, in fresh P72/4 basalt, remanence behaviour appears to be controlled by magnetostriction.

4.2 How does alteration affect the low-temperature magnetism of P72/4 basalt?

A comparison of the magnetic properties of the samples annealed at 355 and 500 or 550 °C shows that the alteration follows significantly different paths depending on the annealing temperature. Annealing at 355 °C produces two magnetic phases with Curie temperatures ranging from 420 °C to approximately 500 °C for phase 1, and about 580–590 °C for minor phase 2. No signs of the Verwey (1939) transition are observed in low-temperature experiments (Figs 7 and 8) ruling out the possibility that phase 2 can be a stoichiometric magnetite. Phase 1 could be either titanomagnetite or titanomaghemite. However, an increase in the Curie temperature by nearly 300 °C would imply a very high degree of oxidation corresponding to values of the oxidation factor $z > 0.8$ (Readman & O'Reilly 1972). Titanomaghemites in this composition range show completely reversible zero-field SIRM cycles between 300 and 5 or

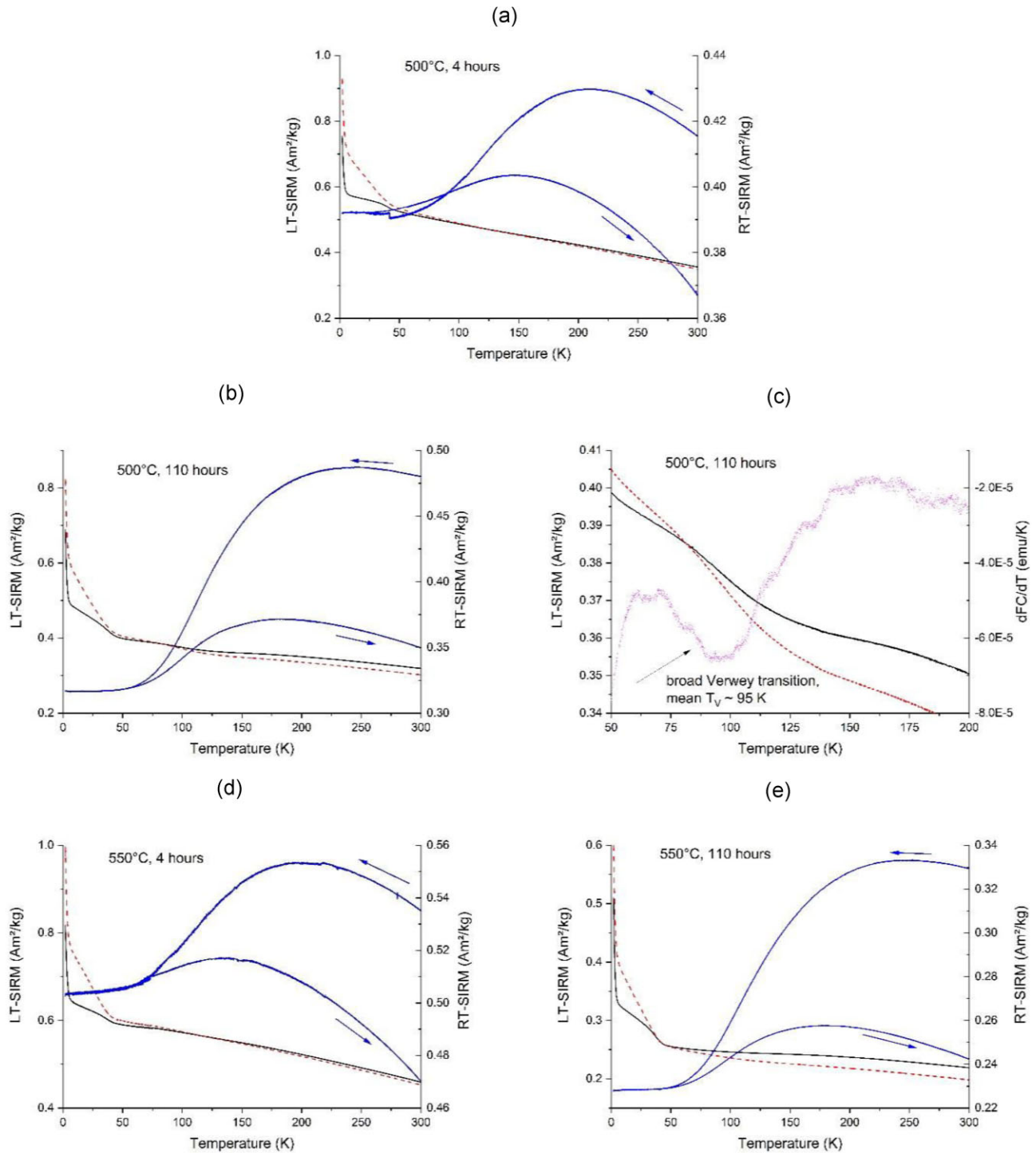


Figure 11. (a) and (b) Decay of SIRM given at 1.8 K after ZFC and FC (5 T), respectively, on warming in a zero field (black and red curves, left ordinate axis), and a zero-field cycle of SIRM given at 300 K (blue curve, right ordinate axis) for samples annealed at 500 °C. Note the different scales on the two ordinate axes. Annealing time is indicated in the figures. Panel (c) displays an enlargement of the plot in panel (b) with overlapped FC derivative curve showing a broad Verwey transition centred at 95 K; and (d) and (e) Same as (a) and (b), but for samples annealed at 550 °C.

10 K, and magnetization may even self-reverse at the lowest temperature (Dobrovine & Tarduno 2004, 2006a,b; Krása & Matzka 2007). In our samples, an entirely different behaviour is observed, with the irreversibility of SIRM cycles increasing with increasing annealing time. This resembles the properties observed in volcanic rocks containing titanomagnetites of TM10–TM30 composition (Kosterov *et al.* 2009, 2018). Therefore, maghemitization does

not appear a viable explanation for the observed low-temperature magnetic properties of annealed P72/4 samples.

Bearing this in mind, we prefer a hypothesis put forward by Bowles and co-authors (Bowles *et al.* 2013, 2019; Jackson & Bowles 2018) that shift of titanomagnetite Curie temperatures to higher values after annealing at a relatively moderate (355 °C) temperature could be at least partly due to increasing ionic order in the

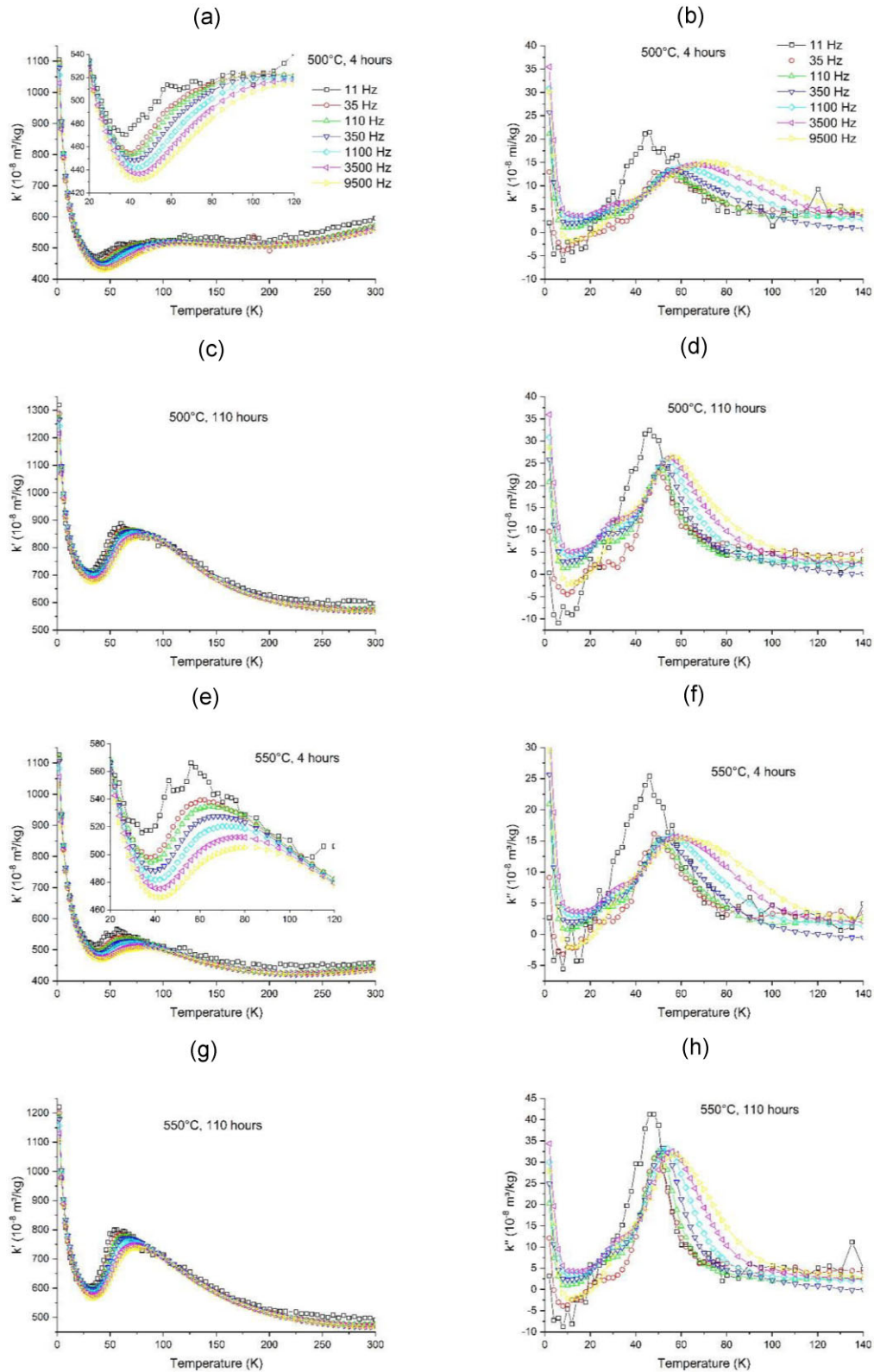


Figure 12. Temperature dependencies of (a), (c), (e) and (g) in-phase and (b), (d), (f) and (h) out-of-phase AC magnetic susceptibility measured at seven frequencies between 11 and 9500 Hz for samples annealed at 500 and 550 °C. Annealing time at 500 °C (a) and (b) 4 hr, and (c) and (d) 110 hr, at 550 °C (e) and (f) 4 hr, and (g) and (h) 110 hr. Out-of-phase susceptibility is essentially constant above 140 K, and so the respective plots are truncated at this temperature to show frequency-dependent behaviour. Insets in (a) and (e) show detailed views of frequency-dependent behaviour of the in-phase susceptibility.

titanomagnetite spinel lattice. Furthermore, this process appears to be reversible to some extent, as indicated by restoring close to original Curie temperatures after heating to 700 °C in an argon atmosphere (Figs 4a–d). For the samples annealed for up to 110 hr, the Curie temperatures deduced from cooling susceptibility versus temperature curves are about 220 °C, and for the sample annealed for 375 hr—260 °C (Fig. 4f). The increase of Curie temperatures of the phase produced by annealing is also accompanied by changes in the shape of temperature dependencies of AC susceptibility at cryogenic temperatures (Fig. 8). At the same time, magnetic softening of titanomagnetite grains occurs with increasing annealing time, as indicated by (i) points in the Day plot moving towards the multidomain (MD) range (Fig. 5), (ii) appearance of MD-like signal in FORC diagrams particularly for the samples annealed for 110 and 375 hr (Figs 6c and d), and (iii) increase of irreversibility of low-temperature zero-field cycles of SIRM given at 300 K (Figs 7a–d). Taken together, these observations further confirm that prolonged annealing at 355 °C results in a considerable lessening of the internal stress in titanomagnetite grains, and magnetostriction becomes less important in controlling remanence properties at cryogenic temperatures.

By contrast, annealing at 500 and 550 °C first produces two magnetic phases with Curie temperatures of about 500 and 560 °C, respectively (Fig. 9). Upon longer (110 hr) annealing, these phases coalesce into a single phase. Interestingly, the Curie temperature of the product phase is somewhat higher (577 °C) for the sample annealed at 500 °C than for the sample annealed at 550 °C (553 °C). The former sample is the only one exhibiting the Verwey transition, characteristic of magnetite with Ti content < 3.5 at. per cent per formula unit (Kozłowski *et al.* 1996); however, even in this sample the signature of the Verwey transition is faint and occurs on the tail of remanence surviving above 40 K. In some cases, further heating to 700 °C in an argon atmosphere during the susceptibility versus temperature experiment produces a Verwey transition-like response in low-temperature susceptibility curves measured after completing the high-temperature cycle (*cf.* Figs 9b and c). The underlying process in both cases appears to be the high-temperature exsolution, similar to that observed in the same basalt cooled from 570 to 569 °C at a rate of 1 °C h⁻¹ and then quickly cooled to room temperature (see Figs 2d and f in Shcherbakov *et al.* 2019). It is worth noting however that the Curie temperature of about 300 °C, which we ascribe to a titanomagnetite phase subjected to a partially reversible ionic reordering, is clearly seen in a susceptibility vs. temperature cooling from 500 °C curve of the fresh sample (Fig. 2b) and in the cooling curve of the sample annealed at 500 °C for 4 hr (Fig. 9f).

At the same time, the general shape of low-temperature remanence (Fig. 11) and AC susceptibility curves (Fig. 12) remain similar to those typical for more Ti-rich intermediate titanomagnetites (Kosterov *et al.* 2009, 2018; Almeida *et al.* 2014). The two most prominent features in remanence curves are: (i) a characteristic triangular shape separating FC and ZFC curves, and (ii) cooling and warming branches of the RT-SIRM zero-field cycle converging between 50–70 K. A possible explanation of this conundrum might be that an exsolved phase with near-magnetite Curie temperatures but without the Verwey transition is a titanomaghemite with both moderate Ti content (say, 0.10–0.15 Ti atoms per formula unit) and a moderate degree of oxidation such as not to modify the behaviour at cryogenic temperatures significantly. If the Curie temperature of this phase and its magnetic hysteresis properties were to be like those of magnetite, it would be impossible to distinguish the two

phases without performing measurements at cryogenic temperatures. A similar explanation may also apply to the absence of the Verwey transition in archaeological ceramics that often contain a magnetically soft phase with Curie temperatures extending up to 560–580 °C (Kosterov *et al.* 2021; Troyano *et al.* 2021).

5 CONCLUSIONS

Comparison of the magnetic properties of basalt samples annealed at 355 and 500 or 550 °C shows that alteration of the initial relatively high-Ti titanomagnetite follows two significantly different paths depending on the annealing temperature, clearly reflected in the magnetic properties of samples at cryogenic temperatures.

In the first case, two magnetic phases are formed with Curie temperatures ranging from 420 to about 500 °C for phase 1 and about 580–590 °C for a minor phase 2. The latter cannot be magnetite because of the absence of a Verwey transition. An increase in the Curie temperature of phase 1 with increasing annealing time is likely associated with an increase in the degree of ionic order in the spinel lattice of titanomagnetite (Bowles *et al.* 2013), and not with maghemitization.

At the initial stage of annealing at 500 and 550 °C, two magnetic phases are formed with Curie temperatures of about 500 and 560 °C, respectively. At a longer (110 hr) annealing, these phases appear to coalesce into a single one. The shape of the low-temperature magnetization and susceptibility curves of the annealed samples is however reminiscent of more Ti-rich titanomagnetites of composition TM10–15, whose Curie temperatures are several tens of degrees lower. The explanation for this discrepancy may be that the phase with a Curie temperature close to magnetite but not showing the Verwey transition is a titanomaghemite with a moderate Ti content and a relatively low degree of oxidation not sufficient to significantly alter the behaviour at cryogenic temperatures characteristic for stoichiometric titanomagnetite.

The results of this study contradict the generally accepted idea that upon the initial stage of annealing, titanomagnetite is oxidized according to a single-phase mechanism, forming titanomaghemite. Indeed, the magnetic properties of highly oxidized titanomaghemites at cryogenic temperatures (Dobrovine & Tarduno 2004, 2006a,b; Krása & Matzka 2007) are known to be entirely different. For moderately oxidized ($z < 0.5$) titanomaghemites, there are practically no data, but it is difficult to envisage a pathway how a sample such as one annealed for 375 hr at 355 °C in this study would, with further oxidation, develop the low-temperature magnetic properties like described by Dobrovine & Tarduno (2004, 2006a; 2006b) and Krása & Matzka (2007). Therefore, we suggest that under ‘dry’ heating conditions, titanomagnetite oxidation does not occur, at least at short timescales, while the corresponding change in magnetic properties is controlled by the reordering of Ti ions in the titanomagnetite lattice (Bowles *et al.* 2013, 2019; Jackson & Bowles 2018).

Overall, the magnetic properties of P72/4 basalt samples annealed for different times at different temperatures show significant variation, resulting from the neoformation of different magnetic phases with distinct Curie temperatures. These results highlight the importance of carefully controlling the heating temperature and time when conducting palaeointensity determinations using conventional methods that involve multiple temperature steps. The occurrence of multiple titanomagnetite and titanomaghemite phases, both original and newly formed, can complicate the interpretation of

palaeointensity data and would require additional analytical techniques to accurately characterize the magnetic properties of the samples.

ACKNOWLEDGMENTS

This study has been supported by Russian Foundation for Basic Research, grants 19–05–00471 to AK and 20–05–00573 to VM. Experimental studies have been performed using the facilities of the Scientific Park of St Petersburg University at the Centre for Diagnostics of Functional Materials for Medicine, Pharmacology and Nanoelectronics, the Centre for Geo-Environmental Research and Modelling (GEOMODEL) and the Centre for Microscopy and Microanalysis. FORC measurements have been carried out at the Institute of Physics of the Earth RAS, Moscow. AK thanks Vladimir Pavlov for hosting his visit, and Pavel Minaev for help with measurements. This paper has benefitted from the reviews by Thomas Berndt and anonymous reviewer, and from editorial comments by Eduard Petrovský.

DATA AVAILABILITY

The data underlying this paper will be shared on reasonable request to the corresponding author.

REFERENCES

- Almeida, T.P., Muxworthy, A.R., Williams, W., Kasama, T. & Dunin-Borkowski, R., 2014. Magnetic characterization of synthetic titanomagnetites: quantifying the recording fidelity of ideal synthetic analogs, *Geochem. Geophys. Geosyst.*, **15**(1), 161–175.
- Aragón, R., Buttrely, D.J., Shepherd, J.P. & Honig, J.M., 1985. Influence of nonstoichiometry on the Verwey transition, *Phys. Rev. B*, **31**, 430–436.
- Bowles, J.A., Jackson, M.J., Berquó, T.S., Solheid, P.A. & Gee, J.S., 2013. Inferred time- and temperature-dependent cation ordering in natural titanomagnetites, *Nat. Commun.*, **4**, 1916. doi:10.1038/ncomms2938.
- Bowles, J.A., Lappe, S.-C.L.L., Jackson, M.J., Arenholz, E. & van der Laan, G., 2019. Curie temperature enhancement and cation ordering in titanomagnetites: evidence from magnetic properties, XMCD, and Mössbauer spectroscopy, *Geochem. Geophys. Geosyst.*, **20**(5), 2272–2289.
- Brown, K. & O'Reilly, W., 1988. The effect of low temperature oxidation on the remanence of TRM-carrying titanomagnetite $\text{Fe}_{2.4}\text{Ti}_{0.6}\text{O}_4$, *Phys. Earth planet. Inter.*, **52**(1–2), 108–116.
- Carter-Stiglitz, B., Moskowitz, B., Solheid, P., Berquó, T.S., Jackson, M. & Kosterov, A., 2006. Low-temperature magnetic behavior of multidomain titanomagnetites: TM0, TM16, and TM35, *J. geophys. Res.*, **111**, B12S05. doi:10.1029/2006JB004561.
- Church, N., Feinberg, J.M. & Harrison, R., 2011. Low-temperature domain wall pinning in titanomagnetite: quantitative modeling of multidomain first-order reversal curve diagrams and AC susceptibility, *Geochem. Geophys. Geosyst.*, **12**(7), Q07Z27.
- Creer, K.M. & Petersen, N., 1969. Thermochemical magnetization in basalts, *Z. Geophys.*, **35**, 501–516.
- Day, R., Fuller, M. & Schmidt, V.A., 1977. Hysteresis properties of titanomagnetites: grain-size and compositional dependence, *Phys. Earth planet. Inter.*, **13**, 260–267. doi:10.1016/0031-9201(77)90108-X.
- Dobrovine, P.V. & Tarduno, J.A., 2004. Self-reversed magnetization carried by titanomaghemite in oceanic basalts, *Earth planet. Sci. Lett.*, **222**(3–4), 959–969.
- Dobrovine, P.V. & Tarduno, J.A., 2005. On the compositional field of self-reversing titanomaghemite: constraints from Deep Sea Drilling Project Site 307, *J. geophys. Res.*, **110**, B11104. doi:10.1029/2005JB003865.
- Dobrovine, P.V. & Tarduno, J.A., 2006a. Alteration and self-reversal in oceanic basalts, *J. geophys. Res.*, **111**, B12S30. doi:10.1029/2006JB004468.
- Dobrovine, P.V. & Tarduno, J.A., 2006b. N-type magnetism at cryogenic temperatures in oceanic basalt, *Phys. Earth planet. Inter.*, **157**(1–2), 46–54.
- Draeger, U., Prévot, M., Poidras, T. & Riisager, J., 2006. Single-domain chemical, thermochemical and thermal remanences in a basaltic rock, *Geophys. J. Int.*, **166**(1), 12–32.
- Dunlop, D.J., 2002. Theory and application of the day plot (M_{rs}/M_s versus H_{cr}/H_c) 1. Theoretical curves and tests using titanomagnetite data, *J. geophys. Res.*, **107**. doi:10.1029/2001JB000486.
- Dunlop, D.J. & Özdemir, Ö., 1997. *Rock Magnetism: Fundamentals and Frontiers*, Cambridge Univ. Press, p. 573.
- Egli, R., 2013. VARIFORC: an optimized protocol for calculating non-regular first-order reversal curve (FORC) diagrams, *Global Planet. Change*, **110**, Part C, 302–320.
- Engelmann, R., Kontny, A. & Lattard, D., 2010. Low-temperature magnetism of synthetic Fe-Ti oxide assemblages, *J. geophys. Res.*, **115**(B12), B12107.
- Fabian, K., 2009. Thermochemical remanence acquisition in single-domain particle ensembles: a case for possible overestimation of the geomagnetic paleointensity, *Geochem. Geophys. Geosyst.*, **10**, Q06Z03. doi:10.1029/2009GC002420.
- Gee, J. & Kent, D.V., 1999. Calibration of magnetic granulometric trends in oceanic basalts, *Earth planet. Sci. Lett.*, **170**, 377–390.
- Gribov, S.K., Shcherbakov, V.P. & Aphinogenova, N.A., 2019. Magnetic properties of artificial CRM created on titanomagnetite-bearing oceanic basalts, in *Recent Advances in Rock Magnetism, Environmental Magnetism and Paleomagnetism*, eds Nurgaliev, D., Shcherbakov, V., Kosterov, A. & Spassov, S. pp. 173–194, Springer International Publishing, Cham.
- Gribov, S.K., Shcherbakov, V.P., Tsel'movich, V.A. & Aphinogenova, N.A., 2021. The properties of thermochemical remanent magnetization acquired by slow laboratory cooling of titanomagnetite-bearing basalt samples from different temperatures and the results of the Thellier method, *Izv. Phys. Solid Earth*, **57**(6), 913–926.
- Heslop, D., Roberts, A.P., Oda, H., Zhao, X., Harrison, R.J., Muxworthy, A.R., Hu, P.-X. & Sato, T., 2020. An automatic model selection-based machine learning framework to estimate FORC distributions, *J. geophys. Res.: Solid Earth*, **125**(10), e2020JB020418.
- Hodych, J.P., 1982a. Magnetostrictive control of coercive force in multidomain magnetite, *Nature*, **298**, 542–544.
- Hodych, J.P., 1982b. Magnetic hysteresis as a function of low temperature for deep-sea basalts containing large titanomagnetite - inference of domain state and controls on coercivity, *Can. J. Earth Sci.*, **19**, 144–152.
- Jackson, M. & Bowles, J., 2018. Malleable Curie temperatures of natural titanomagnetites: occurrences, modes, and mechanisms, *J. geophys. Res.: Solid Earth*, **123**(2), 921–940.
- Johnson, H.P. & Merrill, R.T., 1973. Low-temperature oxidation of a titanomagnetite and the implications for paleomagnetism, *J. geophys. Res.*, **78**, 4938–4949.
- Kakol, Z. & Honig, J.M., 1989. The variation of Verwey transition temperature with oxygen stoichiometry in magnetite, *Solid State Comm.*, **70**, 967–969.
- Kakol, Z., Sabol, J. & Honig, J.M., 1991. Magnetic anisotropy of titanomagnetites $\text{Fe}_{3-x}\text{Ti}_x\text{O}_4$, $0 \leq x \leq 0.55$, *Phys. Rev. B*, **44**, 2198–2204.
- Keefer, C.M. & Shive, P.N., 1980. Titanomaghemites: conditions for oxidation, influence of rhombohedral phases, and temperature of inversion, *Earth planet. Sci. Lett.*, **51**(1), 199–205.
- Keefer, C.M. & Shive, P.N., 1981. Curie temperature and lattice constant reference contours for synthetic titanomaghemites, *J. geophys. Res.*, **86**, 987–998.
- Kellogg, K., Larson, E.E. & Watson, D.E., 1970. Thermochemical remanent magnetization and thermal remanent magnetization; comparison in a basalt, *Science*, **170**, 628–630.

- Klerk, J., Brabers, V.A.M. & Kuipers, A.J.M., 1977. Magnetostriction of the mixed series $\text{Fe}_{3-x}\text{Ti}_x\text{O}_4$, *J. Phys. Coll.*, **38**(C1), C1–187–C1–189.
- Kosterov, A., 2001. Magnetic properties of subaerial basalts at low temperatures, *Earth Planets Space*, **53**, 883–892.
- Kosterov, A. et al. 2021. High-coercivity magnetic minerals in archaeological baked clay and bricks, *Geophys. J. Int.*, **224**(2), 1256–1271.
- Kosterov, A., Conte, G., Goguitchaichvili, A. & Urrutia-Fucugauchi, J., 2009. Low-temperature magnetic properties of andesitic rocks from Popocatepetl stratovolcano, Mexico, *Earth Planets Space*, **61**, 133–142.
- Kosterov, A.A., Sergienko, E.S., Kharitonskii, P.V. & Yu. Yanson, S., 2018. Low temperature magnetic properties of basalts containing near $\sim\text{TM30}$ titanomagnetite, *Izv. Phys. Solid Earth*, **54**(1), 134–149.
- Kozłowski, A., Kąkol, Z., Kim, D., Zaleski, R. & Honig, J.M., 1996. Heat capacity of $\text{Fe}_{3\alpha}\text{M}_\alpha\text{O}_4$ ($\text{M} = \text{Zn}, \text{Ti}, 0 \leq \alpha \leq 0.04$). *Phys. Rev. B*, **54**, 12093–12098.
- Krása, D. & Matzka, J., 2007. Inversion of titanomaghemite in oceanic basalt during heating, *Phys. Earth planet. Inter.*, **160**, 169–179.
- Krása, D., Shcherbakov, V.P., Kunzmann, T. & Petersen, N., 2005. Self-reversal of remanent magnetization in basalts due to partially oxidized titanomagnetites, *Geophys. J. Int.*, **162**(1), 115–136.
- Maksimochkin, V.I. & Grachev, R.A., 2019. The stability of titanomagnetite basalt of the Red Sea during heating in air and argon, *Moscow Univ. Phys. Bull.*, **74**(6), 697–705.
- Maksimochkin, V.I., Grachev, R.A. & Tselebrovskiy, A.N., 2020. Determination of the formation field of artificial CRM and pTRM by the Thellier method at different oxidation stages of natural titanomagnetite, *Izv. Phys. Solid Earth*, **56**(3), 413–424.
- Marshall, M. & Cox, A., 1971. Effect of oxidation on the natural remanent magnetization of titanomagnetite in suboceanic basalt, *Nature*, **230**, 28–31.
- Matzka, J., Krása, D., Kunzmann, T., Schult, A. & Petersen, N., 2003. Magnetic state of 10–40 ma old ocean basalts and its implications for natural remanent magnetization, *Earth planet. Sci. Lett.*, **206**, 541–553.
- Moskowitz, B.M., Jackson, M. & Kissel, C., 1998. Low-temperature magnetic behavior of titanomagnetites, *Earth planet. Sci. Lett.*, **157**, 141–149.
- Muxworthy, A.R., King, J.G. & Odling, N., 2006. Magnetic hysteresis properties of interacting and noninteracting micron-sized magnetite produced by electron beam lithography, *Geochem., Geophys., Geosyst.*, **7**, Q07009. doi:10.1029/2006GC001309.
- Nagata, T. & Kobayashi, K., 1963. Thermo-chemical remanent magnetization of rocks, *Nature*, **197**, 476–477. doi:10.1038/197476a0.
- Nishitani, T. & Kono, M., 1983. Curie temperature and lattice constant of oxidized titanomagnetite, *Geophys. J. R. astr. Soc.*, **74**, 585–600.
- Nishitani, T. & Kono, M., 1989. Effect of low-temperature oxidation on the remanence properties of titanomagnetites, *J. Geomag. Geoelectr.*, **41**, 19–38. doi:10.5636/jgg.41.19.
- Özdemir, Ö. & Dunlop, D.J., 2003. Low-temperature behavior and memory of iron-rich titanomagnetites (Mt. Haruna, Japan and Mt. Pinatubo, Philippines). *Earth planet. Sci. Lett.*, **216**, 193–200.
- Ozima, M. & Larson, E.E., 1970. Low- and high-temperature oxidation of titanomagnetite in relation to irreversible changes in the magnetic properties of submarine basalts, *J. geophys. Res.*, **75**, 1003–1017. doi:10.1029/JB075i005p01003.
- Ozima, M. & Sakamoto, N., 1971. Magnetic properties of synthesized titanomaghemite, *J. geophys. Res.*, **76**, 7035–7046. doi:10.1029/JB076i029p07035.
- Pike, C.R., Roberts, A.P. & Verosub, K.L., 1999. Characterizing interactions in fine magnetic particle systems using first order reversal curves, *J. Appl. Phys.*, **85**, 6660–6667. doi:10.1063/1.370176.
- Radhakrishnamurthy, C. & Likhite, S.D., 1993. Frequency dependence of low-temperature susceptibility peak in some titanomagnetites, *Phys. Earth planet. Inter.*, **76**, 131–135. doi:10.1016/0031-9201(93)90062-E.
- Readman, P.W. & O'Reilly, W., 1972. Magnetic properties of oxidized (cation-deficient) titanomagnetites ($\text{Fe,Ti,}\square$) $_3\text{O}_4$, *J. Geomag. Geoelectr.*, **24**, 69–90. doi:10.5636/jgg.24.69.
- Roberts, A.P., Heslop, D., Zhao, X. & Pike, C.R., 2014. Understanding fine magnetic particle systems through use of first-order reversal curve diagrams, *Rev. Geophys.*, **52**(4), 557–602.
- Schmidbauer, E. & Readman, P.W., 1982. Low temperature magnetic properties of Ti-rich Fe-Ti spinels, *J. Magn. Magn. Mater.*, **27**, 114–118. doi:10.1016/0304-8853(82)90290-6.
- Shaw, J., 1974. A new method of determining the magnitude of the palaeomagnetic field. Application to five historic lavas and five archaeological samples, *Geophys. J. R. astr. Soc.*, **39**, 133–141. doi:10.1111/j.1365-246X.1974.tb05443.x.
- Shcherbakov, V.P., Gribov, S.K., Lhuillier, F., Aphinogenova, N.A. & Tsel'movich, V.A., 2019. On the reliability of absolute palaeointensity determinations on basaltic rocks bearing a thermochemical remanence, *J. geophys. Res.: Solid Earth*, **124**(8), 7616–7632.
- Smirnov, A.V. & Tarduno, J.A., 2005. Thermochemical remanent magnetization in precambrian rocks: are we sure the geomagnetic field was weak?, *J. geophys. Res.*, **110**, B06103. doi:10.1029/2004JB003445.
- Starunov, V.A. et al. 2019. Magnetic properties of tektite-like impact glasses from Zhamanshin astrobleme, Kazakhstan, in *Recent Advances in Rock Magnetism, Environmental Magnetism and Paleomagnetism*, eds Nurgaliev, D., Shcherbakov, V., Kosterov, A. & Spassov, S. pp. 445–465, Springer International Publishing, Cham.
- Surovitskii, L., Makarenko, E., Lukin, M., Smirnov, A.V., Makeev, P. & Alushkin, V., 2022. FORCtool: an online service for rapid analysis of first-order reversal curve (FORC) data, in *AGU Fall Meeting, December 12-16, Chicago IL*, Abstract GP22A-0275. <https://agu.confex.com/agu/fm22/meetingapp.cgi/Paper/1054807>.
- Syono, Y., 1965. Magnetocrystalline anisotropy and magnetostriction of $\text{Fe}_3\text{O}_4\text{-Fe}_2\text{TiO}_4$ series—with special application to rocks magnetism, *Japan. J. Geophys.*, **4**, 71–143.
- Thellier, E. & Thellier, O., 1959. Sur l'intensité du champ magnétique terrestre dans le passé historique et géologique, *Ann. Géophys.*, **15**, 285–376.
- Troyano, M., Gallet, Y., Genevey, A., Pavlov, V., Fournier, A., Lagroix, F., Niyazova, M. & Mirzaakhmedov, D., 2021. Analyzing the geomagnetic axial dipole field moment over the historical period from new archeointensity results at Bukhara (Uzbekistan, Central Asia). *Phys. Earth planet. Inter.*, **310**, 106633. doi:10.1016/j.pepi.2020.106633.
- Verwey, E.J.W., 1939. Electronic conduction of magnetite (Fe_3O_4) and its transition point at low temperatures, *Nature*, **144**, 327–328.
- Vigliotti, L., Bilardello, D., Winkler, A. & Del Carlo, P., 2022. Rock magnetic fingerprint of Mt Etna volcanic ash, *Geophys. J. Int.*, **231**(2), 749–769.
- Waldhaug, H.J., Torsvik, T.H. & Lovlie, R., 1991. Experimental CRM production in a basaltic rock; evidence for stable, intermediate palaeomagnetic directions, *Geophys. J. Int.*, **105**(3), 747–756.
- Walz, F., 2002. The Verwey transition—a topical review, *J. Phys.: Condens. Matter*, **14**, R285–R340. doi:10.1088/0953-8984/14/12/203.
- Wang, S., Chang, L., Tao, C., Bilardello, D., Liu, L. & Wu, T., 2021. Seafloor magnetism under hydrothermal alteration: insights from magnetomineralogy and magnetic properties of the Southwest Indian Ridge basalts, *J. geophys. Res.: Solid Earth*, **126**(12), e2021JB022646.
- Wasilewski, P.J., 1969. Thermochemical remanent magnetization (TCRM) in basaltic rocks experimental characteristics, *J. Geomag. Geoelectr.*, **21**, 595–613. doi:10.5636/jgg.21.595.
- Yamamoto, Y., 2006. Possible TCRM acquisition of the Kilauea 1960 lava, Hawaii: failure of the thellier palaeointensity determination inferred from equilibrium temperature of the Fe-Ti oxide, *Earth Planets Space*, **58**, 1033–1044. doi:10.1186/BF03352608.
- Yamamoto, Y., Tsunakawa, H. & Shibuya, H., 2003. Palaeointensity study of the Hawaiian 1960 lava: implications for possible causes of erroneously high intensities, *Geophys. J. Int.*, **153**, 263–276. doi:10.1046/j.1365-246X.2003.01909.x.